Synthesis, crystal structures and characterization of late first row transition metal complexes derived from benzothiazole core: Anti-tuberculosis activity and special emphasis on…

ARTICLE *in* EUROPEAN JOURNAL OF MEDICINAL CHEMISTRY · MAY 2014

Impact Factor: 3.45 · DOI: 10.1016/j.ejmech.2014.03.083

4 AUTHORS:

Priya Netalkar
Karnatak University, Dharwad
9 PUBLICATIONS **21** CITATIONS
SEE PROFILE

Sandeep Netalkar
Karnatak University, Dharwad
12 PUBLICATIONS **29** CITATIONS
SEE PROFILE

Srinivasa Budagumpi
Jain University
60 PUBLICATIONS **602** CITATIONS
SEE PROFILE

Vidyanand Revankar
Karnatak University, Dharwad
67 PUBLICATIONS **595** CITATIONS
SEE PROFILE

European Journal of Medicinal Chemistry 79 (2014) 47–56

Contents lists available at ScienceDirect

European Journal of Medicinal Chemistry

journal homepage: http://www.elsevier.com/locate/ejmech

Original article

Synthesis, crystal structures and characterization of late first row transition metal complexes derived from benzothiazole core: Anti-tuberculosis activity and special emphasis on DNA binding and cleavage property

Priya P. Netalkar [a], Sandeep P. Netalkar [a], Srinivasa Budagumpi [b], Vidyanand K. Revankar [a,*]

[a] Department of Chemistry, Karnatak University, Pavate Nagar, Dharwad 580 003, Karnataka, India
[b] The School of Chemical Sciences, Universiti Sains Malaysia, 11800 USM, Penang, Malaysia

ARTICLE INFO

Article history:
Received 3 February 2014
Received in revised form
22 March 2014
Accepted 29 March 2014
Available online 31 March 2014

Keywords:
NNO donor ligand
X-ray diffraction
Transition metal complex
DNA binding

ABSTRACT

Air and moisture stable coordination compounds of late first row transition metals, viz. Co(II), Ni(II), Cu(II) and Zn(II), with a newly designed ligand, 2-(2-benzo[d]thiazol-2-yl)hydrazono)propan-1-ol (LH), were prepared and successfully characterized using various spectro-analytical techniques. The molecular structures of the ligand and nickel complex were unambiguously determined by single-crystal X-ray diffraction method. The $[Ni(LH)_2]Cl_2.3H_2O$ complex is stabilized by intermolecular CH···π stacking interactions between the methyl hydrogen and the C18 atom of the phenyl ring (C11—H11B···C18) forming 1D zig-zag chain structure. Both, the ligand and its copper complex, were electrochemically active in the working potential range, showing quasi-reversible redox system. The interactions of all the compounds with calf thymus DNA have been comprehensively investigated using electronic absorption spectroscopy, viscosity, electrochemistry and thermal denaturation studies. The cleavage reaction on pBR322 DNA has been monitored by agarose gel electrophoresis. The results showed that the ligand can bind to CT-DNA through partial intercalation, whereas the complexes bind electrostatically. Further, $[Ni(LH)_2]Cl_2.3H_2O$ and $[CuLCl(H_2O)_2]$ complexes in the series have high binding and cleavage affinity towards pBR322 DNA. Additionally, all the compounds were screened for anti-tuberculosis activity. All the complexes revealed an MIC value of 0.8 μg/mL, which is almost 8 times active than standard used (Streptomycin, 6.25 μg/mL).

1. Introduction

There has been increasing interest in the design of small model molecules that can mimic natural biomolecules, since the interactions of these with DNA helps us to understand how natural biomolecules function in biological systems [1–3]. Design of stable, inert, and non-toxic metal complexes containing spectroscopically active metal centers that read the information in the DNA duplex has been a central goal at the interface of inorganic chemistry and biology. Cisplatin and its derivatives are the most widely used metal-based drugs for cancer therapy, whose modes of actions were determined by their interaction with DNA. However, their use is restricted by serious side effects, general toxicity, and acquired drug resistance [4–7]. These drawbacks drive inorganic chemists to design more effective, cheaper, less toxic, site specific, and preferably non-covalently bound anticancer drugs. A new approach in this task is to examine complexes containing transition metal ions other than platinum. Late first row transition metals viz, cobalt, nickel, copper and zinc are biologically relevant metals as they are associated with various biomolecules related to essential physiological activities. Furthermore, design of metal complexes derived from hydrazine/hydrazone-based ligands have received considerable attention in this area due to their unique ligational properties, significant physicochemical properties and also due to their possible applications as new therapeutic agents [8,9].

In this perspective, benzothiazole anchored hydrazones represent a very interesting class of ligands, due to their additional donor sites; nitrogen and sulfur atoms. Conversely, the biological properties of benzothiazole is often related to metal ion coordination which introduces enhanced synthetic flexibility, selectivity, sensitivity towards the transition metal ions and further the role of metal ion in the complex has its own influence in enhancing the

* Corresponding author.
E-mail address: vkrevankar@rediffmail.com (V.K. Revankar).

http://dx.doi.org/10.1016/j.ejmech.2014.03.083
0223-5234/

overall activity of the complex compared to the free ligand through a synergic effect [10].

In spite of numerous attempts to develop new structural prototype in the search for more effective DNA-targeted guest molecules, benzothiazole still remain as one of the most versatile class of compounds and therefore, are useful substructures for further molecular exploration. Benzothiazole derivatives have attracted continuing interest because of their varied biological activities viz anti-tumor [11,12], anti-tubercular [13,14] anti-malarial [15], anti-convulsant [16], anti-helmintic [17], analgesic [18], anti-inflammtory [19], and anti-diabetic [20].

The present work was undertaken as an attempt to explore the structural relationship of benzothiazole derived hydrazone with late first row transition metal ions and to study the mode of interaction of these metal complexes with DNA. Here we report the synthesis and characterization of the benzothiazole derived ligand, its transition metal complexes including single crystal X-ray structure of the hydrazone and its nickel complex. Further, their binding and cleavage behavior towards calf thymus DNA and pBR322 DNA have been studied by electronic absorption spectroscopy, viscosity, electrochemistry, thermal denaturation studies and agarose gel electrophoresis. A preliminary screening for anti-tubercular activity of these new compounds is also explored.

2. Chemistry

The analytical, physicochemical and electronic spectral parameters of LH and its complexes are compiled in the experimental section. All the complexes are non-hygroscopic and stable to air and moisture at room temperature. They are generally insoluble in water and most organic solvents, like ethanol, methanol, chloroform, benzene and diethyl ether, but are soluble in highly polar organic solvents, like DMF and DMSO. The Ni(II) complex is also soluble in acetonitrile, methanol and ethanol. Analytical and spectroscopic data for the metal complexes indicate a 1:1 (M:L) stoichiometry for $[CuLCl(H_2O)_2]$ and 1:2 for the $[Co(LH)_2]Cl_2$, $[Ni(LH)_2]Cl_2.3H_2O$ and $[Zn(LH)_2]Cl_2$ complexes.

3. Results and discussion

3.1. Infrared spectral studies

The ligand shows broad band at 3346 cm^{-1} attributed to free ν(O–H) vibrations. Further the medium intensity band around 3257 cm^{-1} is assigned to ν(NH), which is also present in all the complexes. A sharp intense band at 1597 cm^{-1} in the ligand is assigned to azomethine ν(C=N). The free ligand also shows a sharp, medium intensity band at 1548 cm^{-1} assigned to the ν(C=N) of the benzothiazole ring. This band has broadened and intensified in all the complexes due to the coupling of exo-azomethine band with azomethine of benzothiazole ring showing a negative shift of about 15–30 cm^{-1}, suggesting coordination of the benzothiazole ring nitrogen and azomethine nitrogen to the central metal ion in all the complexes [21,22]. A sharp intense band at 1020 cm^{-1} in the ligand is assigned to ν(C–O), which has shown positive shift of about 20–35 cm^{-1} in all the complexes indicating the coordination of –OH to the metal ion upon complexation. The Ni(II) complex also show a broad band centred at 3465 cm^{-1} due to presence of water molecules in the complex. Further, the non-ligand bands in the region 520–560 cm^{-1} and 400–490 cm^{-1} are due to the formation of M–O and M–N bonds respectively [23]. In conclusion, these data suggest an ONN tridentate behavior of the ligand.

3.2. ^1H NMR spectral studies

The singlet at 11.10 ppm in the free ligand, ascribed to the hydrazine NH suffered slight downfield shift in the spectrum of $[Zn(LH)_2]Cl_2$, indicating the coordination of azomethine nitrogen to the metal ion. A triplet observed at 5 ppm in the free ligand due to OH proton, appeared as broad singlet in the $[Zn(LH)_2]Cl_2$ spectrum with a downfield shift indicating its involvement in coordination to the metal ion. The aromatic protons resonated as multiplets in the region 7.04–7.60 ppm in the spectrum of ligand, are shifted slightly downfield in the $[Zn(LH)_2]Cl_2$ spectrum. A doublet at 3.97 ppm in the free ligand ascribed to methylene protons appeared as broad singlet and showed a downfield shift in the complex spectrum. The N=C–CH_3 protons are observed as a singlet at 2.01 ppm in the ligand and at 1.96 ppm in the $[Zn(LH)_2]Cl_2$ complex. The proton signals in the aromatic region are discussed in the syntheses section. The ^1H NMR Spectrum of ligand, LH (Fig. S1) and $[Zn(LH)_2]Cl_2$ (Fig. S2) complex are provided in the Supplementary Material.

3.3. Mass and EPR spectral studies

The ESI mass spectrum of $[Ni(LH)_2]Cl_2.3H_2O$ complex is given in Supplementary material (Fig. S3). ESI mass spectral studies of ligand, $[Ni(LH)_2]Cl_2.3H_2O$ and $[CuLCl(H_2O)_2]$ show their molecular ion peaks [M+] at 221, 627 and 356 respectively. On the other hand, the chlorine (^{37}Cl) isotopic peaks, [M+2] and [M+4] in $[Ni(LH)_2]Cl_2.3H_2O$ are seen at 629 and 631 with relatively low intensity, whereas in $[CuLCl(H_2O)_2]$ complex, [M+2] is seen at 358 which evidences the mononuclear structure of the complex. Apart from this, spectrum also shows some additional peaks, which are due to molecular cations of various fragments of the complexes. By comparing the analytical and spectral data of $[Co(LH)_2]Cl_2$ and $[Zn(LH)_2]Cl_2$, relevant structures were assigned for the respective series.

The EPR spectrum of $[CuLCl(H_2O)_2]$ complex was recorded at both room temperature (RT) and liquid nitrogen temperature (LNT). EPR spectrum of $[CuLCl(H_2O)_2]$ is shown in Fig. S4. The $g_{||}$ and $g_{\perp}$ values observed for the complex at LNT are ($g_{||} = 2.28$ and $g_{\perp} = 2.07$) respectively. The trend observed, $g_{||} > g_{\perp} > 2.02$, for the present copper complex is typical of a copper(II) (d^9) ion in axial symmetry with the unpaired electron residing in $d_{x^2-y^2}$ orbital with the possibility of some d_z^2 character being mixed with it because of low symmetry [24]. The $g_{||}$ value ($2.28 < 2.3$) indicates a larger percentage of covalency of metal–ligand bonding [25]. The axial symmetry parameter G is more than 4 rules out the exchange interaction between the copper centers.

3.4. Electronic spectral and magnetic studies

Electronic spectra of the ligand and its complexes were measured in DMF. The free ligand exhibited strong absorptions in the range 250–270 nm due to intra-ligand $\pi \rightarrow \pi^*$ transitions, these bands remain almost unchanged in the spectra of complexes. Absorptions in the range 295–380 nm are attributed to the $n \rightarrow \pi^*$ transition associated with azomethine, the bathochromic shift of this absorption upon complexation is due to the donation of a lone pair of electrons to the metal ion, indicating the coordination of azomethine nitrogen [26,27].

$[Co(LH)_2]Cl_2$ complex possesses a magnetic moment of 4.92 BM, which is in agreement with values reported for three unpaired electrons in an octahedral environment. The lowest energy band at 800 nm was due to $^4T_{1g} \rightarrow {}^4T_{2g}$ (ν_1) and broad band's near 540 and 415 nm were assigned to $^4T_{1g} \rightarrow {}^4A_{2g}$ (ν_2) and $^4T_{1g} \rightarrow {}^4T_{1g}$ (P) (ν_3) transitions respectively, supporting an octahedral geometry for the complex [27]. However, $[Ni(LH)_2]Cl_2.3H_2O$ exhibits a magnetic

moment of 2.96 BM, consistent with octahedral geometry [28]. The electronic spectrum of $[Ni(LH)_2]Cl_2.3H_2O$ displayed d–d transitions around 700, 550 and around 490 nm, assignable to $^3A_{2g} \rightarrow {}^3T_{2g}(\nu_1)$, $^3A_{2g} \rightarrow {}^3T_{1g}(\nu_2)$ and $^3A_{2g} \rightarrow {}^3T_{1g}(P)$ (ν_3) transitions respectively, indicating an octahedral geometry.

The $[CuLCl(H_2O)_2]$ complex in the present study shows a μ_{eff} value of 1.82 B.M, corresponding to one unpaired electron [29]. The absorption spectrum of this complex exhibits broad d–d electronic band centred at 500 nm, assignable to $^2E_g \rightarrow {}^2T_{2g}$ transition [30]. Absorptions in this region are typical of species with octahedral geometry around the Cu(II) ions. Finally, the $[Zn(LH)_2]Cl_2$ complex shows bands at wavelength less than 360 nm, which are due to the intra ligand transitions.

3.5. Thermal analysis

All complexes were studied for their thermal behavior over the temperature range of 25–1000 °C under nitrogen atmosphere. Thermal behavior of $[CuLCl(H_2O)_2]$ and $[Ni(LH)_2]Cl_2.3H_2O$ complexes have been dealt in detail. The spectrum of $[Ni(LH)_2]Cl_2.3H_2O$ is presented as a representative example in supplementary part (Fig. S5). TGA and DTA curves of the $[CuLCl(H_2O)_2]$, indicates that the complex is highly stable up to 170 °C. Further, the complex shows thermal decomposition in three significant steps. The weight loss of 9% in the first step is attributed to the loss of two coordinated water molecules in the region 170–190 °C, further supported by an endothermic signal at 173.8 °C. In the second stage, the decomposition corresponds to a mass loss of 21% in the range 190–270 °C, showing the combined loss of one chloride and the ligand, with the respective DTA curve at 232.3 °C representing an endothermic process. Further reduction of mass in the higher temperature range is ascribed to the decomposition of remaining part of the ligand and finally the graph become plateau because of the formation of stable copper oxide.

The decomposition of $[Ni(LH)_2]Cl_2.3H_2O$ takes place in three stages. The first step of decomposition corresponding to a mass loss of 8.63% in the region 50–90 °C is attributed to the loss of three lattice held water molecules. In the second step, weight loss of 11.32% in the region 200–260 °C corresponds to the loss of two counter chloride ions. Further reduction of mass in the higher temperature range is ascribed to the ligand decomposition and the final product was analyzed to be nickel oxide.

3.6. Single crystal X-ray diffraction study of LH and $[Ni(LH)_2]Cl_2.3H_2O$

A summary of the crystallographic data, bond lengths, and bond angles of LH and $[Ni(LH)_2]Cl_2.3H_2O$ are tabulated in Tables 1–3, respectively. An ORTEP representation of LH and $[Ni(LH)_2]Cl_2.3H_2O$ showing 30% displacement ellipsoids are shown in Figs. 1 and 2, respectively.

Asymmetric unit of LH crystallized in an orthorhombic crystal system with no crystal held solvent or water molecules. Diazine and azomethine modules of the imine maintains coplanarity with the benzothiazole ring, while hydroxyl group makes an dihedral angle of 113.1(3)°. Furthermore, the azomethine, C=N bond (N1–C2), which averages 1.260(4) Å is less than the terminal carbonyl distance, [C3–O1, 1.401(4)] indicating the double bond character, and confirms the formation of azomethine linkage. As expected, the N1–C2 bond length is comparable to the corresponding bond length of 1.26 Å, reported for similar imine molecules [31–34]. The torsion angles −178.8(3)° exhibited by N3–C4–N2–N1 and 2.6(4)° by S1–C4–N2–N1 indicates that N3 and N1 atoms are trans, while S1 and N1 are cis to each other. In the extended crystal structure, imine molecules are connected via C–H···N (2.366 Å) and C–H···O (2.733 Å) hydrogen bonds perpendicular to *ab* and *bc* planes, respectively, forming a three dimensional network. Methyl Hydrogen forms intermolecular π allylic interactions with two atoms [C5 and C10] respectively.

The crystal structure of $[Ni(LH)_2]Cl_2.3H_2O$, consist of $[Ni(LH)_2]^{2+}$ cation along with $2Cl^-$ anions and $3H_2O$ molecules in the outer coordination sphere. The metal centre is coordinated in an N_4O_2

Table 1
Crystal data and structure refinement details of the ligand **LH** and **$[Ni(LH)_2]Cl_2.3H_2O$**.

	LH	$[Ni(LH)_2]Cl_2.3H_2O$
Formula	$C_{10}H_{11}N_3OS$	$C_{20}H_{28}N_6NiO_5S_2$
Formula weight	221.28s	626.21
Crystal system	Orthorhombic	Monoclinic
Space group	*Pca2₁*	*P2₁/c*
Unit cell dimensions		
a (Å)	18.840 (5)	10.093 (5)
b (Å)	10.648 (3)	19.123 (5)
c (Å)	5.123 (10)	14.079 (5)
α (o)	90.00	90.000 (5)
β (o)	90.0	101.314 (5)
γ (o)	90.00	90.000 (5)
V (Å^3)	1027.8 (4)	2664.6 (18)
Z	4	4
Density (calcd) (gm/cm^3)	1.430	1.561
Abs coeff (mm^{-1})	0.290	1.129
F (000)	464	1296
Crystal size (mm)	0.41 × 0.22 × 0.09	0.43 × 0.34 × 0.20
θ Min, max (o)	1.91, 24.06	1.82, 27.31
R (int)	0.0200	0.0357
N_{ref}, N_{par}	1482, 137	5980, 365
R, wR_2, *S*	0.038, 0.098, 1.153	0.041, 0.111, 1.040

Table 2
Selected bond distances (Å) and angles (°) of ligand **LH**.

Bond distance (Å)			
O1–C3	1.401 (4)	C4–N3	1.294 (4)
C3–C2	1.498 (5)	N3–C5	1.396 (4)
C2–N1	1.260 (4)	S1–C6	1.739 (3)
N1–N2	1.392 (4)	C5–C6	1.383 (5)
N2–C4	1.354 (4)	C5–C10	1.394 (5)
C4–S1	1.754 (3)	C6–C7	1.388 (4)
Bond angle (°)			
O1–C3–C2	113.1 (3)	S1–C4–N3	117.2 (2)
C3–C2–N1	116.1 (3)	C4–N3–C5	109.3 (3)
C2–N1–N2	119.0 (3)	C4–S1–C6	87.76 (16)
N1–N2–C4	115.3 (3)	N2–C4–N3	124.8 (3)

Table 3
Selected bond distances (Å) and angles (°) of **$[Ni(LH)_2]Cl_2.3H_2O$**.

Bond distance (Å)			
O1–Ni	2.153 (2)	N1–N2	1.376 (3)
N1–Ni	2.003 (2)	N3–C4	1.301 (3)
N3–Ni	2.052 (2)	N3–C6	1.395 (3)
N4–Ni	2.002 (2)	O2–C13	1.421 (3)
N6–Ni	2.078 (2)	C12–N4	1.272 (3)
O2–Ni	2.117 (2)	N4–N5	1.378 (3)
O1–C3	1.416 (3)	C14–N6	1.302 (3)
C2–N1	1.272 (3)	C14–S2	1.732 (3)
Bond angle (°)			
N1–Ni–N4	171.23 (9)	N3–C4–N2	121.3 (2)
O2–Ni–N6	155.36 (8)	C2–N1–N2	122.9 (2)
O1–Ni–N3	155.85 (8)	C12–N4–N5	122.5 (2)
N1–Ni–O1	76.65 (8)	C4–S1–C5	88.45 (13)
N6–Ni–N3	96.82 (8)	C4–N3–C6	110.7 (2)
N6–Ni–N1	105.12 (9)	S1–C4–N3	117.1 (2)
N1–Ni–O2	99.04 (9)	C14–S2–C20	88.40 (13)
O2–Ni–N4	76.25 (9)	C14–N6–C15	110.3 (2)
N4–Ni–N6	79.16 (9)	N6–C14–S2	117.2 (2)

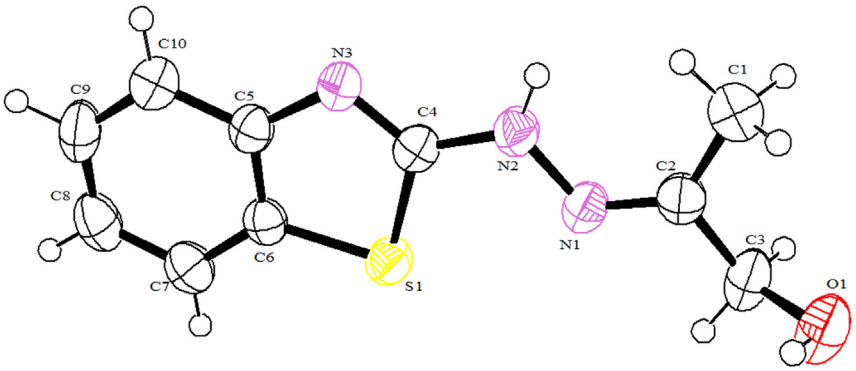

Fig. 1. ORTEP projection of **LH** showing 30% probability ellipsoids.

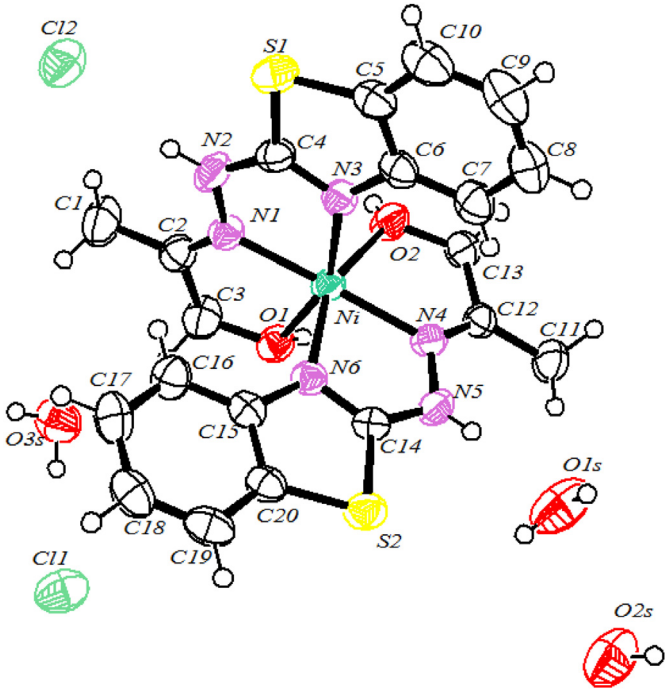

Fig. 2. ORTEP projection of **$[Ni(LH)_2]Cl_2.3H_2O$** showing 30% probability ellipsoids.

core by a tridentate ligand in a meridonial fashion making a dihedral angle of 88.01°, using benzothiazole-N, azomethine-N and hydroxyl-OH atom respectively. The NNO donor sites of the tridentate ligand coordinate the Ni(II) centre to form two five-membered CN_3Ni and C_2NONi chelate rings with bite angles of 79.39(8)° and 76.66(8)° respectively, indicating distortion from an ideal octahedral geometry. The bond distances for Ni–N1, Ni–N6, Ni–O1 and Ni–O2 are 2.003(2), 2.078(2), 2.152(2) and 2.117(2) Ao respectively. Both, the Ni–N and Ni–O, bond distances are in well agreement with the bond distances of similar nickel complexes [33–36]. The average bond lengths in the complex are: N2–N1 = 1.376(3), C4–N2 = 1.363(4), N3–C4 = 1.301(3), N1–C2 = 1.272(4), C2–C3 = 1.494(4), C3–O1 = 1.417(4) Å, which are longer or shorter than those of the corresponding distances in the ligand, LH: N2–N1 = 1.392(4), C4–N2 = 1.354(4), N3–C4 = 1.294(4), N1–C2 = 1.261(4), C2–C3 = 1.499(5), C3–O1 = 1.401(4) Ao and suggest considerable delocalization of the charge on the chelate rings [37]. The intermolecular O–H···O hydrogen bonding, as observed in the free ligand, is absent in the Ni(II) complex due to involvement of the hydroxyl atom in coordination with the Ni(II)centre.

The molecular structure of $[Ni(LH)_2]Cl_2.3H_2O$ is stabilized by many intermolecular hydrogen bonding, N–H···O (2.719 Ao), between N5 hydrogen and the nearby water molecule, N–H···Cl (3.166 Ao), between N2 hydrogen and counter chloride ion respectively, O–H···S (3.227 Ao), between hydroxyl oxygen and benzothiazole-S, O–H···S (2.893 Ao), between benzothiazole-S and nearby water molecule, O–H···Cl (3.103 Ao), between a water molecule and Cl anion, C–H···Cl (2.741 Ao), between methyl hydrogen and counter chloride ion and C–H···O (2.577 Ao), between a methylene hydrogen and nearby water molecule. In addition, the complex molecule is stabilized by intermolecular CH···π stacking interactions between methyl hydrogen and the C18 atom of the phenyl ring (C11–H11B···C18) with a contact distance of 2.812 Å forming a 1D zig-zag chain structure (Fig. S6).

3.7. Cyclic voltammetry studies

The cyclic voltammetric experiments were performed at room temperature in DMF under oxygen free conditions in the potential range −1.0 to +1.0 V, using a glassy carbon working electrode (0.082 cm^2), a platinum counter electrode and an Ag/Ag^+ reference electrode. The redox potential is an important parameter as it characterizes the ability of the redox centre to transfer electrons and also to act as a redox catalyst. The cyclic voltammogram of the ligand was found to be electrochemically active in the working potential range with an anodic and cathodic peak at 0.39 and 0.27 V, respectively. This spectacular behavior of the ligand in the working potential range is attributed to the deprotonation of –OH group of the hydroxy acetone. The difference between anodic and cathodic peak potentials, ΔE_p is more than 59 mV; hence, the redox system is summarized as a quasi-reversible one electron transfer process. The cyclic voltammogram of $[CuLCl(H_2O)_2]$ shows a well-defined redox process corresponding to the Cu(II)/Cu(I) couple. It exhibits a cathodic peak at $E_{pc} = 0.14$ V, corresponding to Cu(II)/Cu(I), and the respective anodic peak for Cu(I)/Cu(II) at $E_{pa} = 0.39$ V. The value of ΔE_p, is more than 59 mV, indicating quasireversible redox process. The dependency of peak potentials on scan rates and value (~ 1) for I_a/I_c (ratio of oxidative to reductive peak currents) indicates simple one-electron transfer [38]. Remaining complexes did not show any electrochemical response over the working potential range.

4. Biochemistry

4.1. DNA binding/cleavage studies

4.1.1. Absorption studies

Electronic absorption spectroscopy is an effective method to examine the binding modes of the metal complexes with DNA. The extent of hypochromism generally indicates an intercalative

binding strength. The hyperchromic effect might be ascribed to external contact (electrostatic binding) or to partial uncoiling of the helix structure of DNA, exposing more bases of the DNA. The absorption titrations of the free ligand, LH and its complexes in the absence and presence of CT-DNA were recorded. LH exhibited hypochromism around 300 nm ($K_b = 0.37 \times 10^4$), while remaining complexes exhibited both hypo and hyperchromism. For $[Ni(LH)_2]Cl_2.3H_2O$ (Fig. 3), the broad band around 490 nm showed a marked hyperchromism with blue shift of ~6–8 nm, accompanied by an isosbestic point at 491 nm and hypochromism around 300 nm with an isobestic point at 308 nm. In $[Co(LH)_2]Cl_2$, the broad band around 410 nm showed marked hyperchromism along with hypochromism at 260 nm with the formation of isobestic point at 305 nm, ($K_b = 1.16 \times 10^4$) (Fig. S7). $[CuLCl(H_2O)_2]$ complex showed marked hyperchromism around 500 nm and hypochromism around 300 nm with isobestic point at 243 nm. Finally, $[Zn(LH)_2]Cl_2$ complex showed marked hyperchromism around 335 nm and hypochromism around 290 nm with isobestic point at 305 nm ($K_b = 1.49 \times 10^3$) (Fig. S8). These observations are indicative of both electrostatic and hydrophobic interactions.

The hyperchromic effect may be due to the electrostatic interaction between positively charged $[M(L)_2]^{2+}$ complex unit and the negatively charged phosphate backbone at the periphery of the double-helix CT-DNA [39] and hypochromism observed may be due to the presence of aromatic chromophore which might facilitate the interaction of the complexes with the CT-DNA bases through non-covalent π–π interactions [40]. By observing the intrinsic binding constants of ligand and complexes, it has been suggested that nickel ($K_b = 2.31 \times 10^4$) and copper ($K_b = 1.72 \times 10^4$) complexes showed greater binding properties.

4.1.2. Viscosity studies

As a means for further clarifying the binding nature of complexes with CT-DNA, the viscosity of CT-DNA solutions containing varying amounts of added complexes were measured. Hydrodynamic measurements that are sensitive to the length change (i.e., viscosity and sedimentation) are regarded as the least ambiguous and the most critical investigations to determine the binding model in solution in the absence of crystallographic structural data. A conventional intercalation mode of binding generally results in lengthening of the DNA helix as base pairs are separated to accommodate the binding agent, leading to an increase of DNA viscosity. Conversely, a partial or non-classical intercalation of binding agent may bend (or kink) the DNA helix, resulting in a decrease of its effective length and, concurrently, its viscosity [41]. The relative viscosity of CT-DNA increases with increase in the concentration of the ligand, LH which is ascribed to the intercalative binding mode, whereas the complexes showed decrease (Fig. 4) in viscosity with relative increase in the their concentrations. Further, these observations are consistent with thermal denaturation studies. From the viscosity studies, it can be concluded that ligand binds to CT-DNA through partial intercalation, whereas the complexes bind electrostatically.

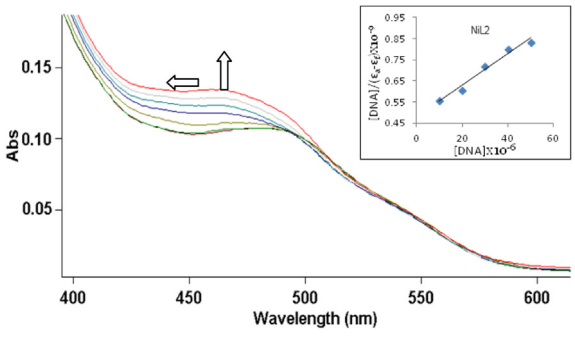

Fig. 3. Absorption spectrum of **$[Ni(LH)_2]Cl_2.3H_2O$** (30 μM) in the absence and presence (10, 20, 30, 40, 50 μM, respectively) of CT-DNA. The arrow shows the absorbance changes upon the increasing of CT-DNA concentrations. Inset plots of $[DNA]/(\varepsilon_f - \varepsilon_a)$ versus [DNA].

4.1.3. Cyclic voltammetry studies

Cyclic voltammetry is also a useful technique for investigating the interaction of metal complexes with DNA [42]. In the absence of CT-DNA, the ligand showed an oxidation peak at 0.39 V and respective reduction peak at 0.28 V. After interaction with 100 μL CT-DNA, ligand experiences a negative shift in $E_{1/2}$ by about 0.03 V as well in E_p values as shown in Fig. 5a. In the absence of CT-DNA, the electrochemical behavior of the $[CuLCl(H_2O)_2]$ showed a redox process, corresponding to Cu(II)/Cu(I) couple. On addition of CT-DNA, the complex also experiences a negative shift in $E_{1/2}$ as well in E_p values as shown in Fig. 5b [43]. In addition to the changes in formal peak potentials, the voltammetric peak decreases upon addition of CT-DNA in both the ligand and copper complex, suggesting their interaction with CT-DNA. The decrease in the current is due to the diffusion of the equilibrium mixture of free and DNA-bound metal complex to the electrode surface [44]. Based on electrochemical studies, it has been concluded that both ligand and $[CuLCl(H_2O)_2]$ complex, bind to CT-DNA via electrostatic mode. But these results totally did not complement with absorption studies. Therefore, in order to better understand the binding behavior, spectroscopic, viscosity and thermal denaturation studies were undertaken.

4.1.4. Thermal denaturation studies

Thermal behavior of CT-DNA in the presence of the metal complexes has also been studied. Stability of the DNA double helix influences the melting temperature (T_m) of CT-DNA, while the binding of compounds to CT-DNA alters the T_m, depending on the strength of interactions. Intercalation of small molecules into the double helix is known to increase the helix melting temperature (T_m), the temperature at which the double helix denatures into single-stranded DNA. The extinction coefficient of CT-DNA bases at 260 nm in the double-helical form is much less than in the single-stranded form; therefore, melting of the helix leads to an increase in the absorption at this wavelength. Melting curves of CT-DNA in the absence and presence of complexes are shown in Fig. 6. The T_m of CT-DNA, in the absence of any added complex was found to be

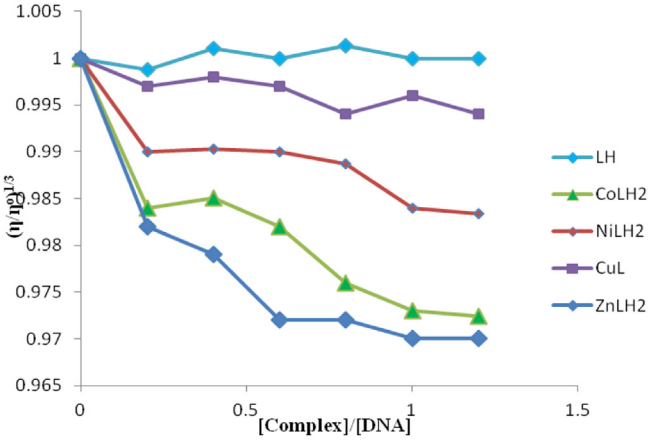

Fig. 4. Effect of increasing amounts of **LH** and its complexes on the relative viscosities of CT-DNA.

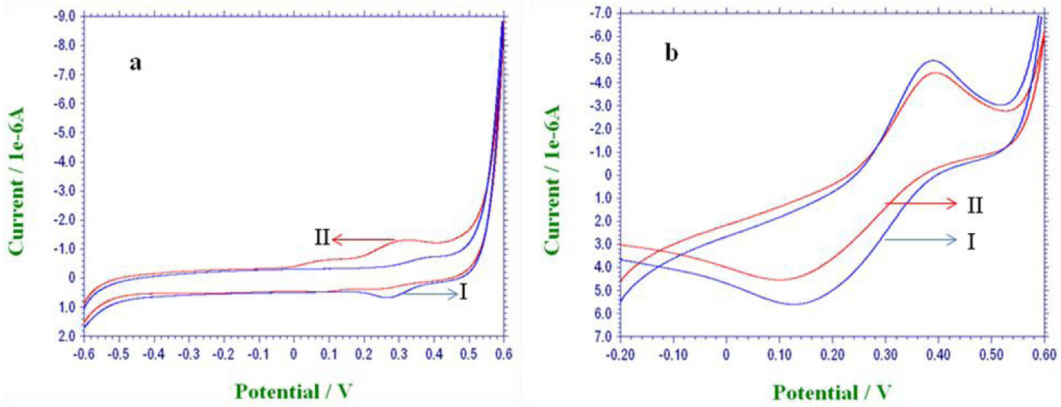

Fig. 5. Cyclic voltammograms of **LH** (5a) and **[CuLCl(H$_2$O)$_2$]** (5b) in the absence (I) and presence (II) of 100 μM CT-DNA in Tris–HCl of pH 7.4 (scan rate = 50 mV s^{-1}).

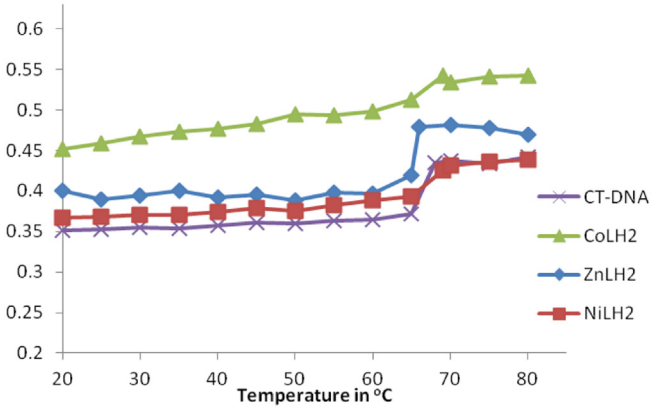

Fig. 6. Melting curves of CT-DNA in the absence and presence of **[Co(LH)$_2$]Cl$_2$**, **[Ni(LH)$_2$]Cl$_2$.3H$_2$O** and **[Zn(LH)$_2$]Cl$_2$** complexes.

68 °C under our experimental conditions. Under the same set of conditions, ligand LH showed hypercromicity with increased T_m of 71 °C ($\Delta T_m = +3$ °C) indicative of the partial intercalation of aromatic chromophore between the DNA base pairs causing stabilization of the base stack, whereas in the case of complexes viz., [Co(LH)$_2$]Cl$_2$, T_m of 69 ($\Delta T_m = +1$ °C), [Ni(LH)$_2$]Cl$_2$.3H$_2$O, T_m of 69 ($\Delta T_m = +1$ °C), [CuLCl(H$_2$O)$_2$], T_m of 69 ($\Delta T_m = +1$ °C) and [Zn(LH)$_2$]Cl$_2$, T_m of 66 ($\Delta T_m = -2$ °C), negligible or lower ΔT_m (C) values are indicative of their non-intercalative mode of binding with CT-DNA.

4.1.5. DNA cleavage study by gel electrophoresis

The cleavage of pBR322 DNA has been monitored by agarose gel electrophoresis. When electrophoresis is applied to circular plasmid DNA, a fastest migration will be observed for DNA of closed circular conformations (Form I). If one strand is cleaved, the supercoil will relax to produce a slower-moving nicked conformation (Form II). If both strands are cleaved, a linear conformation (Form III) will be generated that migrates in between [45]. Fig. 7 shows the results of cleaving super helical plasmid pBR322 DNA induced by interaction with the ligand and its complexes. It has been observed from gel electrophoresis that Form I plasmid DNA, seen in case of ligand is gradually converted into Form II in case of [Co(LH)$_2$]Cl$_2$ and [Zn(LH)$_2$]Cl$_2$. In case of [Ni(LH)$_2$]Cl$_2$.3H$_2$O and [CuLCl(H$_2$O)$_2$], the nicked DNA degraded completely into small pieces and only smear was present. These results suggest that ligand and its complexes can cleave pBR322 DNA, to different degrees. Futher, [Ni(LH)$_2$]Cl$_2$.3H$_2$O and [CuLCl(H$_2$O)$_2$] complexes have shown greater cleavage potential compared to ligand and other complexes studied.

4.2. anti-tubercular activity

All the synthesized compounds were evaluated for their anti-mycobacterial activity against *M. tuberculosis* using microplate Alamar Blue assay (MABA). The data is tabulated in Table 4, which revealed that the metal complexes showed better anti-tubercular activity than ligand with MIC of 0.8 μg/mL compared to standard streptomycin (MIC 6.25 μg/mL).

5. Experimental

5.1. Materials and physical measurements

All the reagents were commercially available (Aldrich) and were used as supplied. Solvents were purified and dried according to standard procedures. 2-hydrazinobenzothiazole was prepared according to the standard procedures reported elsewhere [46]. The zinc chloride used was anhydrous whereas the other metal salts were in their hydrated form, i.e., CoCl$_2$.6H$_2$O, NiCl$_2$.6H$_2$O and CuCl$_2$.2H$_2$O. The metal content of the complexes was determined according to standard methods [47]. The ^{1}H NMR spectrum of the

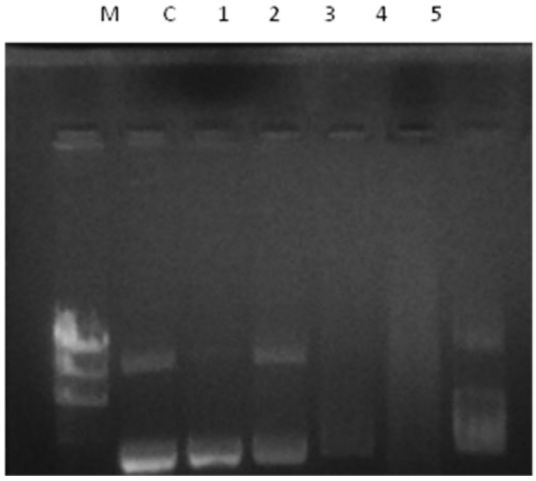

Fig. 7. Photograph of gel electrophoresis experiment of **LH** series on pBR322 DNA. lane M, DNA marker; lane C, untreated DNA; lane 1, **LH**; lane 2, **[Co(LH)$_2$]Cl$_2$**; lane 3, **[Ni(LH)$_2$]Cl$_2$.3H$_2$O**; lane 4, **[CuLCl(H$_2$O)$_2$]**; lane 5, **[Zn(LH)$_2$]Cl$_2$**.

Table 4
Results of anti-tubercular activity of compounds MICs (μg/mL).

Compounds	Anti-tubercular activity
LH	1.6
$[Co(LH)_2]Cl_2$	0.8
$[Ni(LH)_2]Cl_2.3H_2O$	0.8
$[CuLCl(H_2O)_2]$	0.8
$[Zn\ (LH)_2]Cl_2$	0.8
Streptomycin	6.25

ligand was recorded on a BRUKER 300 MHz spectrometer, while ^1H NMR spectrum of the Zn(II) complex and ^{13}C NMR spectrum of ligand on a BRUKER 400 MHz spectrometer in DMSO-d_6 with tetramethylsilane (TMS) as an internal standard. The molar conductivity was measured on an ELICO-CM-82 conductivity bridge. Infrared spectra of the ligand and its metal complexes were recorded in KBr discs in the region 4000–400 cm^{-1} on a Nicolet 170 SX FT-IR spectrometer. The magnetic susceptibility measurements were made on Faraday balance at room temperature using Hg $[Co(SCN)_4]$ as calibrant. All the compounds were analyzed for carbon, hydrogen and nitrogen using a Thermo quest elemental analyzer. The UV–Vis spectra of all the compounds in DMF were recorded on a Varian Cary 50 Bio UV–Vis spectrophotometer. Thermal analysis of the metal complexes were carried out on a Universal V2.4F TA instrument, keeping the final temperature at 1000 °C and the heating rate maintained at 10 °C/min. The cyclic voltammetric experiments were carried out with a three electrode apparatus using a CHI1110A electrochemical analyzer (USA). Electron paramagnetic resonance (EPR) spectrum of the Cu(II) complex was recorded at both room temperature and LNT on a Varian E-4 X-band spectrometer using tetracyanoethylene (TCNE) as the g-marker. The Ostwald viscometer was used for hydrodynamic measurements.

The X-ray diffraction data were obtained at 293 K on a Bruker SMART APEX2 CCD area-detector diffractometer using a graphite monochromated Mo-Kα (k = 0.71073 Å) radiation source. The frames were integrated with the Bruker SAINT Software package using a narrow-frame algorithm. The structures were solved by direct methods, and refined by full-matrix least-square on F^2. Each hydrogen atom was placed in a calculated position, and refined using a riding model. All non-hydrogen atoms were refined anisotropically. Structure solution and refinement were performed using SHELXL-97 package [48]. Structure figures were generated with ORTEP-III [49].

5.2. Synthesis of 2-(2-benzo[d]thiazol-2-yl)hydrazono)propan-1-ol [LH]

The ligand was prepared in two steps. First, 2-hydrazinobenzothiazole was obtained and purified by the literature method [46]. In the second step, hydroxy acetone (0.074 g, 1 mmol) was added dropwise to a 20 mL methanolic solution of 2-hydrazinobenzothiazole (0.165 g, 1 mmol) and the mixture was stirred for 4 h at room temperature (Scheme 1). The completeness of the reaction was monitored through TLC by the consumption of reactants. The yellow colored precipitate formed was set aside for 1 h, then filtered and washed with cold methanol. The solid product was dried *in vacuo* for 4 h. Yellow colored crystals, suitable for single crystal X-ray diffraction analysis, were obtained by slow evaporation of its methanolic solution.

Yield 78%; m.p. 149–151 °C; Color: yellow. ^1H NMR (DMSO-d_6) δ: 11.10 (s, 1H, N_2H) (D_2O exchange), 5.08 (t, 1H, OH, J = 5.9 Hz) (D_2O exchange), 3.97 (d, 2H, C_3H_2, J = 5.9 Hz), 2.01 (s, 3H, $C1H_3$), 7.04 (dd, 1H, J = 7.6 Hz, J = 7.6 Hz, C_8H aromatic), 7.23 (dd, 1H, J = 7.6 Hz, J = 7.6 Hz, C_9H aromatic), 7.36 (d, 1H, J = 7.7 Hz, C_7H aromatic), 7.60 (d, 1H, J = 7.7 Hz, $C_{10}H$ aromatic). Anal. Calc. for LH (%): C, 54.28; H, 5.01; N, 18.99; O, 7.23; S, 14.49. Found: C, 54.00; H, 5.05; N, 18.70; O, 7.00; S, 14.35. FTIR (in cm^{-1}): ν(C=N) 1597; benzothiazole ring, ν(C=N) 1548; hydrazine, ν(NH) 3257 and 3164; ν(C–O) 1020. λ_{max} (in nm): 250 π–π* and 295 n-π*.

5.3. Syntheses of metal complexes

A methanolic solution of the $CuCl_2.2H_2O$ (1 mmol) was added dropwise to the solution of ligand in methanol (0.221 g, 1 mmol) and stirred for 4 h at room temperature. The precipitate obtained was filtered off, washed with cold methanol and dried *in vacuo*. Co(II), Ni(II) and Zn(II) complexes were obtained by refluxing the respective metal chlorides with methanolic solution of ligand for 3–4 h. The product obtained was filtered off, washed several times with methanol, and dried *in vacuo*. Brown colored crystals of $[Ni(LH)_2Cl_2](3H_2O)$, suitable for single crystal X-ray diffraction analysis, were obtained by slow evaporation of its methanolic solution. Attempts to grow single crystals of the remaining metal complexes were unsuccessful. Schematic representation for the syntheses of complexes is shown in Scheme 2.

5.3.1. $[Co(LH)_2]Cl_2$

Color: Reddish brown, Yield: 65%. μ_{eff}: 4.92 BM. Anal. Calc. for $C_{20}H_{22}Cl_2CoN_6O_2S_2$: C, 41.97; H, 3.87; N, 14.68; O, 5.59; S, 5.59; Cl, 12.39; Co, 10.30%. Found: C, 41.03; H, 3.54; N, 14.32; O, 5.20; S, 5.23; Cl, 12.12; Co, 10.14%. IR (cm^{-1}): hydrazine, ν(NH) 3313; benzothiazole ring, ν(C=N) 1539, ν(C–O) 1047. λ_{max} (nm): 240, 280 π–π*, 326 n-π*, 415, 540, 800 (d–d transition). Molar conductivity ($ohm^{-1}\ cm^2\ mol^{-1}$): 235.

5.3.2. $[Ni(LH)_2]Cl_2.3H_2O$

Color: Brown, Yield: 70%. μ_{eff}: 2.96 BM. Anal. Calc. for $C_{20}H_{28}Cl_2NiN_6O_5S_2$: C, 38.36; H, 4.51; N, 13.42; O, 12.77; S, 10.24; Cl, 11.32; Ni, 9.37%. Found: C, 38.20; H, 4.40; N, 13.37; O, 12.50; S, 10.20; Cl, 11.22; Ni, 9.29%. IR (cm^{-1}): hydrazine, ν(NH) 3321; benzothiazole ring, ν(C=N) 1520, ν(C–O) 1054. λ_{max} (nm): 257 π–π*, 335 n-π*, 490, 550, 700 (d–d transitions). Molar conductivity ($ohm^{-1}\ cm^2\ mol^{-1}$): 230. The single crystal structure of the complex was further confirmed by XRD.

5.3.3. $[CuLCl(H_2O)_2]$

Color: Brown, Yield: 73%. μ_{eff}: 1.82 BM. Anal. Calc. for $C_{10}H_{14}CuClN_3O_3S$: C, 33.80; H, 3.97; N, 11.83; O, 13.51; S, 9.00; Cl, 9.98; Cu, 17.89%. Found: C, 33.18; H, 3.60; N, 11.23; O, 13.09; S, 9.02; Cl, 9.87; Cu, 17.78%. IR (cm^{-1}): hydrazine, ν(NH) 3305; benzothiazole ring, ν(C=N) 1538, ν(C–O) 1050. λ_{max} (nm): 250 π–π*, 338 n-π*, 500 (d–d transition). Molar conductivity ($ohm^{-1}\ cm^2\ mol^{-1}$): 34.5.

5.3.4. $[Zn(LH)_2]Cl_2$

Color: yellow, Yield: 65%. ^1H NMR (DMSO-d6) δ: 11.19(s, 1H, N_2H), 5.1(D_2O exchange) (bs, 1H, OH), 4.0(bs, 2H, C_3H_2), 1.96(s, 3H, C_1H_3), 7.06(dd, 1H, J = 7.6 Hz, J = 7.6 Hz, C_8H aromatic) 7.26(dd, 1H, J = 7.6 Hz, J = 7.6 Hz, C_9H aromatic), 7.37(d, 1H, J = 7.7 Hz, C_7H aromatic), 7.7(d, 1H, J = 7.7 Hz, $C_{10}H$ aromatic). Anal. Calc. for $C_{20}H_{22}Cl_2ZnN_6O_2S_2$: C, 41.50; H, 3.83; N, 14.52; O, 5.53; S, 11.08; Cl, 12.25 Zn, 11.29%. Found: C, 41.44; H, 3.7; N, 14.43; O, 5.43; S, 10.57; Zn, 11.22%. IR (cm^{-1}): hydrazine, ν(NH) 3137; benzothiazole ring, ν(C=N) 1532, ν(C–O) 1040. λ_{max} (nm): 250 π–π*, 338 n-π*. Molar conductivity ($ohm^{-1}\ cm^2\ mol^{-1}$): 230.

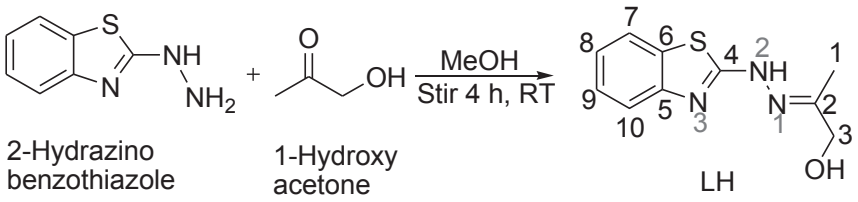

Scheme 1. Synthetic route for the preparation of ligand LH.

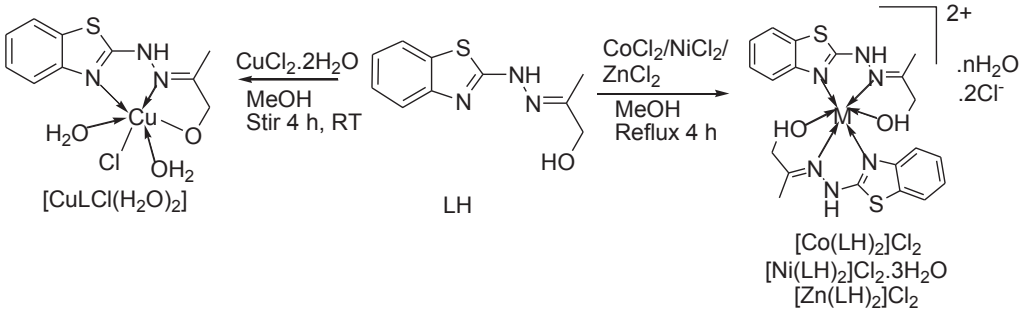

Scheme 2. Synthetic route for the preparation of complexes.

5.4. Biochemistry

5.4.1. DNA interaction studies

The concentration of CT-DNA per nucleotide [C(p)] was measured by using its known extinction coefficient at 260 nm (~6600 M^{-1} cm^{-1}). Tris buffer [5 mM tris (hydroxymethyl)aminomethane, pH 7.2, 50 mM NaCl] was used for the absorption, viscosity and electrochemistry experiments. The absorbance at 260 nm (A260) and at 280 nm (A280) for CT-DNA was measured to check its purity. The ratio A260/A280 was found to be 1.2, indicating that CT-DNA was satisfactorily free from protein. The spectroscopic titrations were carried out by adding increasing amounts of CT-DNA (10, 20, 30, 40, 50 μM) to a solution of the complex at a fixed concentration (30 μM) contained in a quartz cell. In constructing the UV-visible spectrophotometric DNA titration curves, the DNA absorption was subtracted. In order to evaluate quantitatively the DNA-binding strength, the intrinsic DNA-binding constant K_b, was derived by nonlinear regression analysis using equation (1) [50,51].

$$[\mathrm{DNA}]/(\varepsilon_a - \varepsilon_f) = [\mathrm{DNA}]/(\varepsilon_b - \varepsilon_f) + [1/K_b(\varepsilon_b - \varepsilon_f)] \quad (1)$$

Where, [DNA] is the concentration of CT-DNA per base pairs, ε_a is the apparent absorption coefficient, which was obtained by calculating A_{abs}/[complex], and ε_f and ε_b are the extinction coefficients for the free complex and complex in the fully bound form, respectively. In plots of [DNA]/($\varepsilon_a - \varepsilon_f$) vs. [DNA]. K_b is given by the ratio of slope to the intercept.

Thermal denaturation studies were carried out on a UV-visible spectrometer equipped with temperature-controlling thermostat by monitoring the absorption of CT-DNA (60 μM in phosphate buffer at pH 6.8 (μ = 0.2 mol l^{-1} M NaCl) at 260 nm at various temperatures, both in the presence (5–10 μM) and absence of each complex. The temperature was scanned from 25 °C to 80 °C. The melting temperature (T_m) was taken as the midpoint of the hyperchromic transition [50,51].

Viscosity measurements were carried out using an Oswald micro-viscometer maintained at a constant temperature (26.0 ± 0.1 °C) in a thermostat. The CT-DNA concentration was kept constant in all samples (100 μM), but the complex concentration was increased each time (from 50 to 200 μM). Mixing of the solution was achieved by bubbling nitrogen gas through the viscometer. The flow time was measured with a digital stop watch. The sample flow times were measured three times and the mean value was considered for calculation. Data are presented in a plot of $(\eta/\eta_o)^{1/3}$ versus the ratio [complex]/[DNA], where η and η_o are the specific viscosity of CT-DNA in presence and in absence of the complex, respectively. The values of η and η_o were calculated by using the equation:

$$\eta = (t - t_o)/t_o$$

Where, 't' is the observed flow time of a solution containing CT-DNA and the complexes and 't_o' is the flow time of the CT-DNA solution alone. The relative viscosities for CT-DNA were calculated from the relation (η/η_o) [52].

The cyclic voltammetric experiments were carried out with a three electrode apparatus using a CHI1110A electrochemical analyzer (USA). The complexes were dissolved in DMF to the desired concentrations. Cyclic voltammograms of fixed concentrations of the complexes (1 mmol/L) in the absence and presence of CT-DNA (100 μM) were measured. The shifts in the values of ΔEp (separation of the anodic and cathodic peak potentials), i_{pc}/i_{pa} (the ratio of the cathodic to anodic peak currents), and the formal potential $E_{1/2}$ explains the binding ability of the complexes with CT-DNA.

5.4.2. Nuclease activity using gel electrophoreses

For the gel electrophoresis experiments [53], solutions of the complexes in DMF (1 mg/mL) were prepared and these test samples (1 μg) were added to the genomic DNA samples of pBR322 and incubated for 2 h at 37 °C. Agarose gel was prepared in TAE buffer (4.84 g Tris base, pH 8.0, 0.5 M EDTA/l pH 7.3), the solidified gel obtained at ~55 °C was placed in an electrophoresis chamber flooded with TAE buffer. Then 20 μL each of the incubated complex-DNA mixtures (mixed with bromophenol blue dye at a 1:1 ratio) was loaded on the gel along with the standard DNA marker, and the electrophoresis was carried out under the TAE buffer system at 50 V for 2 h. At the end of the electrophoresis, the gel was carefully

stained with EtBr (ethidium bromide) solution (10 μg/mL) for 10–15 min and visualized under UV light using a Bio-Rad Trans illuminator. The illuminated gel was photographed by using a Polaroid camera (a red filter and Polaroid film were used).

5.4.3. Anti-tubercular activity using Alamar Blue Dye [54]

The antimycobacterial activities of compounds were assessed against *M. tuberculosis* ATTC 27294 using microplate Alamar Blue assay (MABA). This methodology is non-toxic, uses a thermally stable reagent and shows good correlation with proportional and BACTEC radiometric method. Briefly, 200 μL of sterile deionized water was added to all outer perimeter wells of sterile 96 wells plate to minimize the evaporation of medium in the test wells during incubation. The 96 wells plate received 100 μL of the Middlebrook 7H9 broth and serial dilution of compounds were made directly on plate. The final drug concentrations tested were 100 to 0.2 μg/mL. Plates were covered and sealed with parafilm and incubated at 37 °C for five days. After this time, 25 μL of freshly prepared 1:1 mixture of Almar Blue reagent and 10% tween 80 was added to the plate and incubated for 24 h. A blue color in the well was interpreted as no bacterial growth, and pink color was scored as growth. The MIC was defined as lowest drug concentration which prevented the color change from blue to pink.

6. Conclusions

In the present work cobalt(II), nickel(II), copper(II) and zinc(II) complexes of a new analog of benzothiazole were designed and synthesized in good yield. The benzothiazole Schiff base binds the metal centre through benzothiazole-N, azomethine-N and hydroxyl-OH atom respectively. Analytical and spectroscopic data for the metal complexes indicate a 1:1 (M:L) stoichiometry for $[CuLCl(H_2O)_2]$ and 1:2 for the remaining complexes under study. The EPR spectrum of $[CuLCl(H_2O)_2]$ complex at LNT, indicates an axial symmetry, with the unpaired electron lying in the $d_{x^2-y^2}$ orbital with the possibility of some d_z^2 character being mixed with it because of low symmetry. The molecular structure of $[Ni(LH)_2]Cl_2.3H_2O$ complex, reveals that the metal centre is coordinated in an N_4O_2 core by a tridentate ligand in a meridonial fashion, and adopts a distorted octahedral geometry. The complex is stabilized by intermolecular CH···π stacking interactions between methyl hydrogen and the C18 atom of the phenyl ring (C11–H11B···C18) forming 1D zig-zag chain structure. Both, the ligand and copper complex, were electrochemically active in the working potential range, showing quasi-reversible redox system. The experimental results showed that the ligand can bind to CT-DNA through partial intercalation, whereas the complexes bind electrostatically, as the non-planar configuration in these, makes it difficult to intercalate within the base pairs of DNA. Further, $[Ni(LH)_2]Cl_2.3H_2O$ and $[CuLCl(H_2O)_2]$ complexes in the series have high binding and cleavage affinity towards pBR322 DNA which is further confirmed by the gel electrophoresis study. Additionally, all the compounds were screened for anti-tuberculosis activity. The ligand LH and its complexes revealed an MIC value of 0.8 μg/mL, which is almost 8 times active than standard used (Streptomycin, 6.25 μg/mL).

Acknowledgments

The authors thank USIC, Karnatak University, Dharwad, for providing spectral facilities. Recording of EPR and IR spectra from IIT-Bombay is gratefully acknowledged. One of the authors (Sandeep P. Netalkar) is thankful to Department of Science & Technology for providing financial assistance under INSPIRE fellowship program.

Appendix A. Supplementary data

Supplementary data related to this article can be found at http://dx.doi.org/10.1016/j.ejmech.2014.03.083.

References

[1] K.H. Thompson, C. Orvig, Dalton Transactions 6 (2006) 761–764.
[2] H. Xu, Y. Liang, P. Zhang, F. Du, B.R. Hou, J. Wu, J.H. Liu, Journal of Biological Inorganic Chemistry 10 (2005) 529–538.
[3] Y.M. Song, Q. Wu, P.J. Yang, N.N. Luan, L.F. Wang, Y.M. Liu, Journal of Inorganic Biochemistry 100 (2006) 1685–1691.
[4] B. Rosenberg, L.V. Camp, J.E. Trosko, V.H. Mansour, Nature 222 (1969) 385–386.
[5] E.R. Jamieson, S.J. Lippard, Chemical Reviews 99 (1999) 2467–2498.
[6] Z. Wu, Q. Liu, X. Liang, X. Yang, N. Wang, X. Wang, H. Sun, Y. Luand, Z. Guo, Journal of Biological Inorganic Chemistry 14 (2009) 1313–1323.
[7] Y. Jung, S.J. Lippard, Chemical Reviews 107 (2007) 1387–1407.
[8] M.P. Sathisha, S. Budagumpi, N.V. Kulkarni, G.S. Kurdekar, V.K. Revankar, K.S.R. Pai, European Journal of Medicinal Chemistry 45 (2010) 106–113.
[9] N. Raman, J.D. Raja, A. Sakthivel, Journal of Chemical Sciences 119 (2007) 303–310.
[10] P.P. Netalkar, A. Kamath, S.P. Netalkar, V.K. Revankar, Spectrochimica Acta, Part A 97 (2012) 762–770.
[11] A. Weekes, A.D. Westwell, Current Medicinal Chemistry 16 (2009) 2430–2440.
[12] J. Lion, C.S. Matthews, G. Wells, T.D. Bradshaw, M.F.G. Stevens, A.D. Westwell, Bioorganic & Medicinal Chemistry Letters 16 (2006) 5005–5008.
[13] Y. Cho, T.R. Ioerger, J.C. Sacchettini, Journal of Medicinal Chemistry 51 (2008) 5984–5992.
[14] Q. Huang, J. Mao, B. Wan, Y. Wang, R. Brun, Journal of Medicinal Chemistry 52 (2009) 6757–6767.
[15] A. Burger, S.N. Sawhey, Journal of Medicinal Chemistry 11 (1968) 270–273.
[16] R.D. Chakole, N.D. Amnerkar, P.B. Khedekar, K.P. Bhusari, Indian Journal of Heterocyclic Chemistry 15 (2005) 27–30.
[17] N.D. Amnerkar, K.P. Bhusari, Journal of Enzyme Inhibition and Medicinal Chemistry 26 (2011) 22–28.
[18] N. Siddiqui, M. Alam, A.A. Siddiqui, Asian Journal of Chemistry 16 (2004) 1005–1008.
[19] S.K. Srivastava, R. Yadav, S.D. Srivastava, Indian Journal of Chemistry 43 (2004) 399–405.
[20] H.M. Diaz, R.V. Molina, R.O. Andrade, D.D. Coutino, L.M. Franco, S.P. Webster, M. Binnie, S.E. Soto, M.I. Barajas, I.L. Rivera, G.N. Vazquez, Bioorganic & Medicinal Chemistry Letters 18 (2008) 2871–2877.
[21] S. Budagumpi, V.K. Revankar, Transition Metal Chemistry 35 (2010) 649–658.
[22] D.X. West, A.A. Nassar, F.A. El-Saied, M.I. Ayad, Transition Metal Chemistry 23 (1998) 423–427.
[23] K. Nakamato, Infrared and Raman Spectra Of Inorganic and Coordination Compounds, Wiley Interscience, New York, 1971.
[24] B.J. Hathway, D.E. Billing, Coordination Chemistry Reviews 5 (1970) 143–207.
[25] D. Kivelson, R. Neiman, Journal of Chemical Physics 35 (1961) 149–155.
[26] L. Antolini, L. Menabue, G.C. Pellacani, M. Saladin, L.P. Batuglia, A.B. Corradi, G. Marcotrigian, Journal of the Chemical Society Dalton Transactions (1984) 2325–2326, http://dx.doi.org/10.1039/DT9840002325.
[27] S. Budagumpi, M.P. Sathisha, N.V. Kulkarni, G.S. Kurdekar, V.K. Revankar, Journal of Inclusion Phenomena and Macrocyclic Chemistry 66 (2010) 327–333.
[28] A.B.P. Lever, Inorganic Electronic Spectroscopy, second ed., Elsevier, Amsterdam, 1984.
[29] B.N. Figgis, J. Lewis, in: J. Lewis, R.G. Wilkins (Eds.), Modern Coordination Chemistry: Principles and Methods, Interscience, New York, 1960.
[30] N. Raman, S. Ravichandran, C. Thangaraja, Journal of Chemical Sciences 116 (2004) 215–219.
[31] X.G. Zhou, J.S. Huang, X.Q. Yu, Z.Y. Zhou, C.M. Che, Journal of the Chemical Society Dalton Transactions (2000) 1075–1080, http://dx.doi.org/10.1039/A908917I.
[32] C.M. Che, J.S. Huang, Coordination Chemistry Reviews 242 (2003) 97–113.
[33] R.N. Patel, V.P. Sondhiya, D.K. Patel, K.K. Shukla, Y. Singh, Indian Journal of Chemistry 51 (2012) 1695–1700.
[34] A. Majumder, G.M. Rosair, A. Mallick, N. Chattopadhyay, S. Mitra, Polyhedron 25 (2006) 1753–1762.
[35] M.C. Aragoni, M. Arca, S.L. Coles, F.A. Devillanova, M.B. Hursthouse, F. Isaia, V. Lippolis, Dalton Transactions 41 (2012) 6611–6613.
[36] A. Datta, H. Jui-Hsien, B. Machura, Journal of Chemical Crystallography 42 (2012) 691–696.
[37] J.R. Dilworth, J. Hyde, P. Lyford, P. Vella, K. Venkatasubramanian, J.A. Zubieta, Inorganic Chemistry 18 (1979) 268–274.
[38] H. Okawa, M. Tadokoro, Y. Aratake, M. Ohba, K. Shindo, M. Mitsumi, M. Tomono, D.E. Funton, Journal of the Chemical Society Dalton Transactions (1993) 253–258, http://dx.doi.org/10.1039/DT9930000253.
[39] N. Shahabadi, S. Mohammadi, Bioinorganic Chemistry and Applications 2012 (2012) 8.

[40] Q.X. Wang, K. Jiao, F.Q. Liu, X.L. Yuan, W. Sun, Journal of Biochemical and Biophysical Methods 70 (2007) 427–433.
[41] L.X. Wen, Z.Y. Jun, L.Y. Tuan, W.Z. Yong, Y.C. Wei, European Journal of Medicinal Chemistry 46 (2011) 3851–3857.
[42] Q.X. Wang, F. Gao, K. Jiao, Electroanal 19 (2008) 2096–2101.
[43] M.T. Carter, A.J. Bard, Journal of the American Chemical Society 111 (1989) 8901–8911.
[44] N. Raman, A. Selvan, P. Manisankar, Spectrochimica Acta, Part A 76 (2010) 161–173.
[45] Y. Li, Y. Wu, J. Zhao, P. Yang, Journal of Inorganic Biochemistry 101 (2007) 283–290.
[46] (a) V.K. Revankar, V.H. Arali, V.B. Mahale, Indian Journal of Chemistry 29 (1990) 889–894;
(b) A. Rutavicius, S. Iokubaitite, Khimiya Geterotsiklicheskikh Soedinenii 1 (1984) 4.
[47] A.I. Vogel, A Textbook of Quantitative Inorganic Analysis, third ed, ELBS, Longman, London, UK, 1961.
[48] G.M. Sheldrick, SHELXS-97, Program for Crystal Structure Solution, Universität Gçttingen, Gçttingen, 1997.
[49] M.N. Burnett, C.K. Johnson, ORTEP-III: Oak Ridge Thermal ellipsoid plot program for Crystal structure Illustrations, Oak Ridge National Laboratory Report ORNL-6895, 1996.
[50] M.N. Patel, P.A. Dosi, B.S. Bhatt, Applied Organometallic Chemistry 25 (2011) 653–660.
[51] Y.M. Chen, A.G. Zhang, K.Z. Wang, Applied Organometallic Chemistry 25 (2011) 521–525.
[52] R. Palchaudhuri, P.J. Hergenrother, Current Opinion In Biotechnology 18 (2007) 497–503.
[53] A. Arslantas, A.K. Devrim, H. Necefoglu, International Journal of Molecular Sciences 8 (2007) 564–571.
[54] M.C.S. Lourenço, M.V.N. de Souza, A.C. Pinheiro, M.L. Ferreira, R.S.B. Gonçalves, T.C.M. Nogueira, M.A. Peraltab, Arkivoc 15 (2007) 181–191.